Acetyl-CoA carboxylase 1 depletion suppresses *de novo* fatty acid synthesis and mitochondrial β-oxidation in castration-resistant prostate cancer cells

Shaoyou Liu[1,‡], Jiarun Lai[2,‡], Yuanfa Feng[2,‡], Yangjia Zhuo[3,‡], Hui Zhang[3], Yupeng Chen[2], Jinchuang Li[3], Xinyue Mei[4], Yanting Zeng[5], Jiaming Su[6], Yulin Deng[2], Funeng Jiang[3], Shengbang Yang[3], Huijing Tan[3], Chi Tin Hon[7], Sun Wei[8], Zhaodong Han[3,*], Fen Wang[9,*], and Weide Zhong[1,2,3,7,8,*]

From the [1]Guangdong Provincial Institute of Nephrology, Nanfang Hospital, Southern Medical University, Guangzhou, China; [2]Department of Urology, Guangdong Key Laboratory of Urology, The First Affiliated Hospital of Guangzhou Medical University, Guangzhou Medical University, Guangzhou, Guangdong, China; [3]Department of Urology, Guangdong Key Laboratory of Clinical Molecular Medicine and Diagnostics, Guangzhou First People's Hospital, School of Medicine, South China University of Technology, Guangzhou, China; [4]State Key Laboratory of Respiratory Disease & National Clinical Research Center for Respiratory Disease, Guangzhou Institute of Respiratory Health, The First Affiliated Hospital of Guangzhou Medical University, Guangzhou Medical University, Guangzhou, China; [5]Guangzhou First People's Hospital, School of Medicine, South China University of Technology, Guangzhou, China; [6]Department of Urology, Guangzhou Baiyun District Women and Children's Hospital, Guangzhou, Guangdong, China; [7]Macau Institute for Applied Research in Medicine and Health, Macau University of Science and Technology, Taipa, Macau, China; [8]The Central Laboratory, Affiliated Huadu Hospital, Southern Medical University, Guangzhou, Guangdong, China; [9]Center for Translational Cancer Research Institute of Biosciences and Technology Texas A&M University, Houston, Texas, USA

Edited by Eric Fearon

Cancer cells, including those of prostate cancer (PCa), often hijack intrinsic cell signaling to reprogram their metabolism. Part of this reprogramming includes the activation of *de novo* synthesis of fatty acids that not only serve as building blocks for membrane synthesis but also as energy sources for cell proliferation. However, how *de novo* fatty acid synthesis contributes to PCa progression is still poorly understood. Herein, by mining public datasets, we discovered that the expression of acetyl-CoA carboxylase alpha (ACACA), which encodes acetyl-CoA carboxylase 1 (ACC1), was highly expressed in human PCa. In addition, patients with high ACACA expression had a short disease-free survival time. We also reported that depletion of ACACA reduced *de novo* fatty acid synthesis and PI3K/AKT signaling in the human castration-resistant PCa (CRPC) cell lines DU145 and PC3. Furthermore, depletion of ACACA downregulates mitochondrial beta-oxidation, resulting in mitochondrial dysfunction, a reduction in ATP production, an imbalanced $NADP^+$/NADPhydrogen(H) ratio, increased reactive oxygen species, and therefore apoptosis. Reduced exogenous fatty acids by depleting lipid or lowering serum supplementation exacerbated both shRNA depletion and pharmacological inhibition of ACACA-induced apoptosis *in vitro*. Collectively, our results suggest that inhibition of ectopic ACACA, together with suppression of exogenous fatty acid uptake, can be a novel strategy for treating currently incurable CRPC.

According to the statistics of 36 cancers in 185 countries, the incidence of prostate cancer (PCa) is 14.1% and the mortality rate is 6.8%, which ranks as the second most common and fifth most deadly cancer in men (1). The latest released data estimate that nearly 270 thousand cases of PCa will be diagnosed yearly in the United States, ranking PCa the first male cancer incidence and the fifth leading cause of cancer death (2). At the early stage, PCa is an indolent disease that grows slowly. However, PCa progresses quickly once it enters advanced and symptomized stages. Radical resection with androgen deprivation follow-up therapies is the first-line treatment for PCa. Most PCa eventually progress to metastatic androgen treatment-resistant disease called metastatic castration-resistant PCa (mCRPC) (3). Although extensive progress has been made in PCa management (4), there is still no cure for mCRPC. Therefore, it remains urgent to develop more effective strategies for the early diagnosis, treatment, and prevention of mCRPC.

Cancer cells often hijack cell signaling to reprogram the metabolism to support their fast growth (5, 6). Emerging evidence shows that abnormal fatty acid metabolism in cancer cells promotes cancer progression by providing crucial fatty acids needed for membrane synthesis, cell signaling, energy, and NADPH production (7). There are three main sources of fatty acids in cancer cells: (1) exogenous intake of fatty acids, (2) lipolysis, and (3) *de novo* fatty acid synthesis from acetyl-CoA (8). Unlike most normal human cells, which obtain fatty acids through exogenous pathways, cancer cells depend on *de novo* synthesis (9). Therefore, hyperactivated *de novo* fatty acid synthesis has become a metabolic feature of many

cancer types, including PCa, which is regarded as a promising target for cancer treatment (7, 10–13).

The rate-limiting enzyme in fatty acid *de novo* synthesis is acetyl-CoA carboxylase 1 (ACC1, encoded by acetyl-CoA carboxylase alpha (ACACA)), which catalyzes acetyl-CoA carboxylation to form malonyl-CoA. Both acetyl-CoA and malonyl-CoA are substrates for long-chain fatty acid synthesis (14). Therefore, targeting ACACA to inhibit *de novo* fatty acid synthesis has been tested in multiple types of cancer, including lung cancer cells, breast cancer, and hepatocellular carcinoma (15–17). However, in other cases, inhibition of ACACA has been shown to promote cancer cell survival and metastasis (18, 19). Interestingly, depletion of ACACA by siRNA in LNCaP cells decreases proliferation and increases apoptosis (20) but not in benign human BPH-1 cells or normal human skin fibroblasts. Recently, we also discovered that the inhibition of ACACA in CRPC cells led to mitochondrial damage and suppressed cell proliferation both *in vivo* and *in vitro* (21). However, it is still unclear how *de novo* synthesis of fatty acids contributes to CRPC cell metabolism and how it contributes to cancer cell progression in CRPC cells. Furthermore, how mCRPC cells escape ACACA depletion is also unknown. To address this unmet challenge, we depleted ACACA expression in the androgen-independent CRPC cell lines DU145 and PC3. We found that depletion of ACACA reduced *de novo* fatty acid synthesis and PI3K/AKT signaling, downregulated mitochondrial beta-oxidation, resulting in mitochondrial dysfunction, and induced apoptosis, which was exacerbated by reducing exogenous fatty acids. The results suggest that inhibition of ectopic ACACA, together with suppression of exogenous fatty acid uptake, can be a novel strategy for treating currently uncurable CRPC.

Results

ACACA is highly expressed in PCa, and its expression level is associated with low disease-free survival

First, we analyzed the public PCa dataset to mine the key abnormally expressed molecules related to the *de novo* fatty acid synthesis pathway in human PCa. In addition to the hallmark fatty acid metabolism gene set downloaded from the gene set enrichment analysis (GSEA) database (gsea-msigdb. org), we also identified 87 key genes that were most relevant to *de novo* fatty acid synthesis. Next, we downloaded multiple datasets containing PCa samples and noncancer prostate tissues from the Gene Expression Omnibus (GEO) database, including the Taylor dataset (150 cases of cancer and 29 cases of noncancer), The Cancer Genome Atlas (TCGA) (492 cases of cancer and 52 cases of noncancer), and GSE70768 dataset (125 cases of cancer and 74 cases of noncancer). We identified 40, 23, and 41 significantly differentially expressed fatty acid metabolism–related genes from the aforementioned datasets, respectively. Among these genes, 14 genes overlapped. Among these 14 genes, the expression of eight genes was increased in cancer tissues and the expression of the other six was reduced (Fig. 1, A−C). We then assessed how the expression levels of these genes were related to the clinical outcome of PCa. TCGA database profiling from GEPIA2 (http://gepia2.cancer-pku.cn/

#index) showed that none of these 14 genes had an impact on the overall survival of PCa. However, the expression levels of four genes (ACACA, ACSL3, SLC27A2, ACADVL) were found to be significantly related to disease-free survival (DFS) time (Fig. 1, D–G). Higher expression of ACSL3 and SLC27A2 was accompanied by higher DFS, while higher expression of ACACA and ACADVL was accompanied by lower DFS. Furthermore, analyses of the TCGA pancancer database (http://ualcan.path.uab.edu) revealed that the expression of ACACA in PCa was the highest among all cancer types (Fig. S1A). Consistently, ACACA expression in PCa cells was the highest at both the mRNA and protein levels compared with all cell types in the Cancer Cell Line Encyclopedia (CCLE) database (https://portals.broadinstitute.org/ccle) (Fig. S1, B and C). Furthermore, analyses of the Grasso dataset (61 cases of cancer and 34 cases of noncancer) and Lapointe dataset (71 cases of cancer and 41 cases of noncancer) in the Oncomine database also revealed that ACACA was highly expressed in PCa (Fig. 1, H–I). Consistent with the mRNA expression level, immunochemical staining of PCa and its adjacent noncancerous tissues demonstrated that PCa had a higher ACACA expression than adjacent noncancerous prostate tissue at the protein level (Fig. S1D). As 27 cases mCRPC and 49 cases localized samples are including in the GSE35988 dataset, we further analyzed and found that mCRPC had a high ACACA expression than the localized ones (Fig. 1J). Together, our findings suggest that ACACA is a potential target for suppressing *de novo* fatty acid synthesis in PCa.

Depletion of ACACA in CRPC cells reduces fatty acid content and suppresses β-oxidation in the mitochondria

ACACA is the rate-limiting enzyme of *de novo* fatty acid synthesis and plays a crucial role in PCa initiation. To determine how ACACA contributes to the fatty acid metabolism of CRPC cells, shRNA was employed to deplete ACACA in DU145 and PC3 cells through stable transfection. Western blot analyses showed that the expression of ACACA was depleted at both the mRNA and protein levels (Figs. 2A and 4, S−T). Consistently, the cellular fatty acid content was reduced in ACACA-depleted cells (Fig. 2B). Next, metabolomics was employed to profile the global change in ACACA-depleted cells. The abundance of 39 metabolites was found to be significantly changed in ACACA-depleted cells. We then analyzed the upregulated and downregulated metabolite profiles separately with a public metabolic bioinformatics analysis website (https://www.metaboanalyst.ca/). The results showed changes in 50 metabolic pathways. However, only the fatty acid metabolism pathway and the mitochondrial beta-oxidation of the long-chain fatty acid pathway were significantly downregulated (Fig. 2, C−D). Furthermore, to discover the potential biological pathways related to ACACA in PCa, seven public datasets (Cambridge, CancerMap, GSE21019, GSE25136, GSE29079, GSE54460, GSE8218) were fitted into GSEA. The result showed that pathways related to fatty acid metabolism and fatty acid beta-oxidation were statistical significance and pathway activated (Fig. 2E).
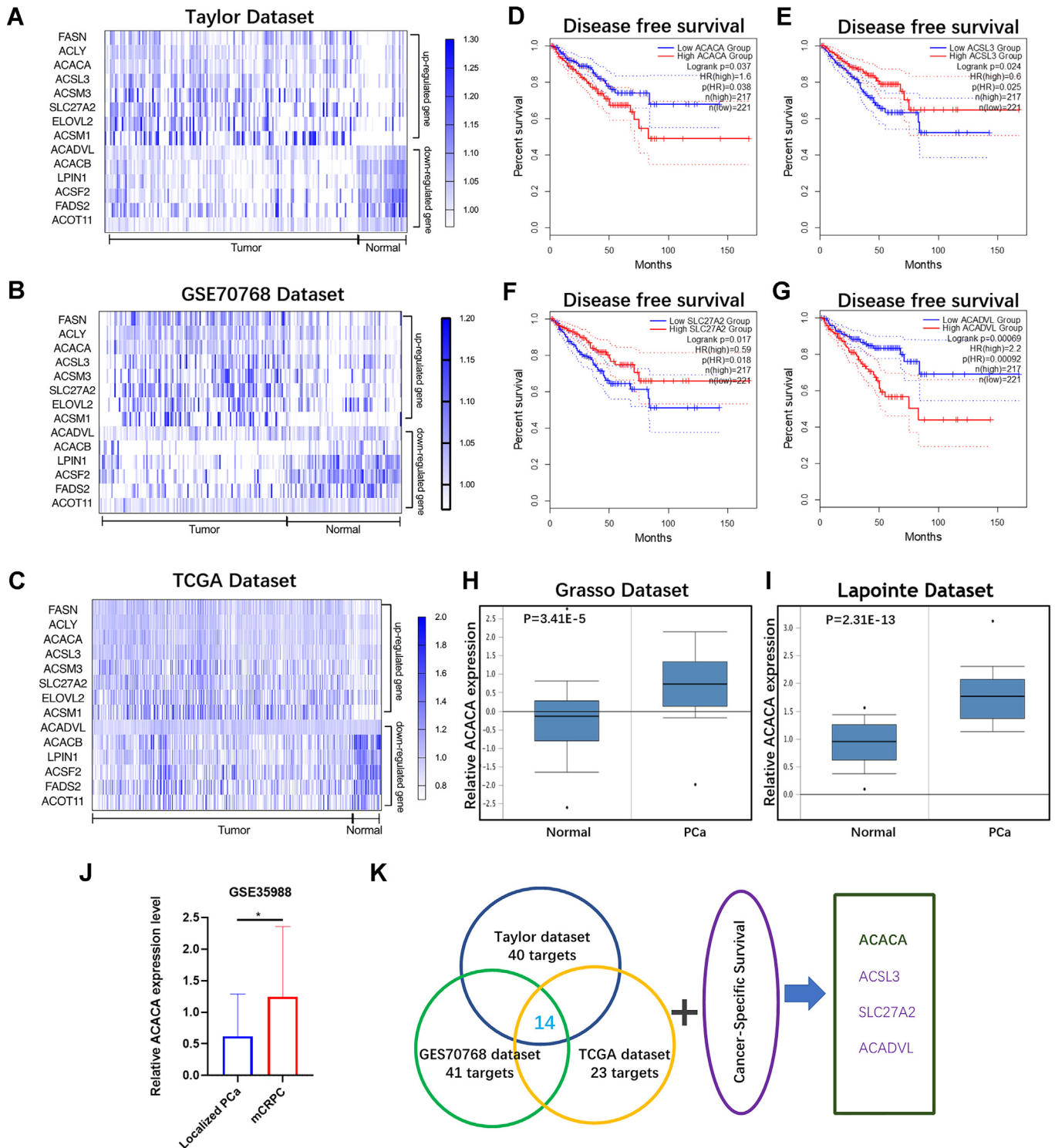
Figure 1. High ACACA expression is associated with a shorter disease-free survival time. *A–C,* expression profiles of 14 key fatty acid metabolism genes in the indicated PCa databases (Taylor GSE70768 TCGA, respectively). *D–G,* disease-free survival time is significantly associated with ACACA, ACSL3, SLC27A2, and ACDVL expression levels in PCa patients. *H* and *I,* relative ACACA expression in the indicated dataset. *J,* representative images of immunohistochemistry staining of ACACA in the PCa tissue microarray. *K,* Venn diagram model of the specific process in obtaining ACACA as the target gene. **p* < 0.05.

Depletion of ACACA inhibits de novo **fatty acid synthesis and PI3K/AKT signaling in CRPC cells**

To explore the role of ACACA in the cellular network, we profiled the cellular molecular interactions of ACACA with the String and Pathway Common database (https://string-db.org and https://apps.pathwaycommons.org). The STRING database showed that 10 molecules had a close relationship with ACACA (Fig. 3A), which were all *de novo* fatty acid synthesis–
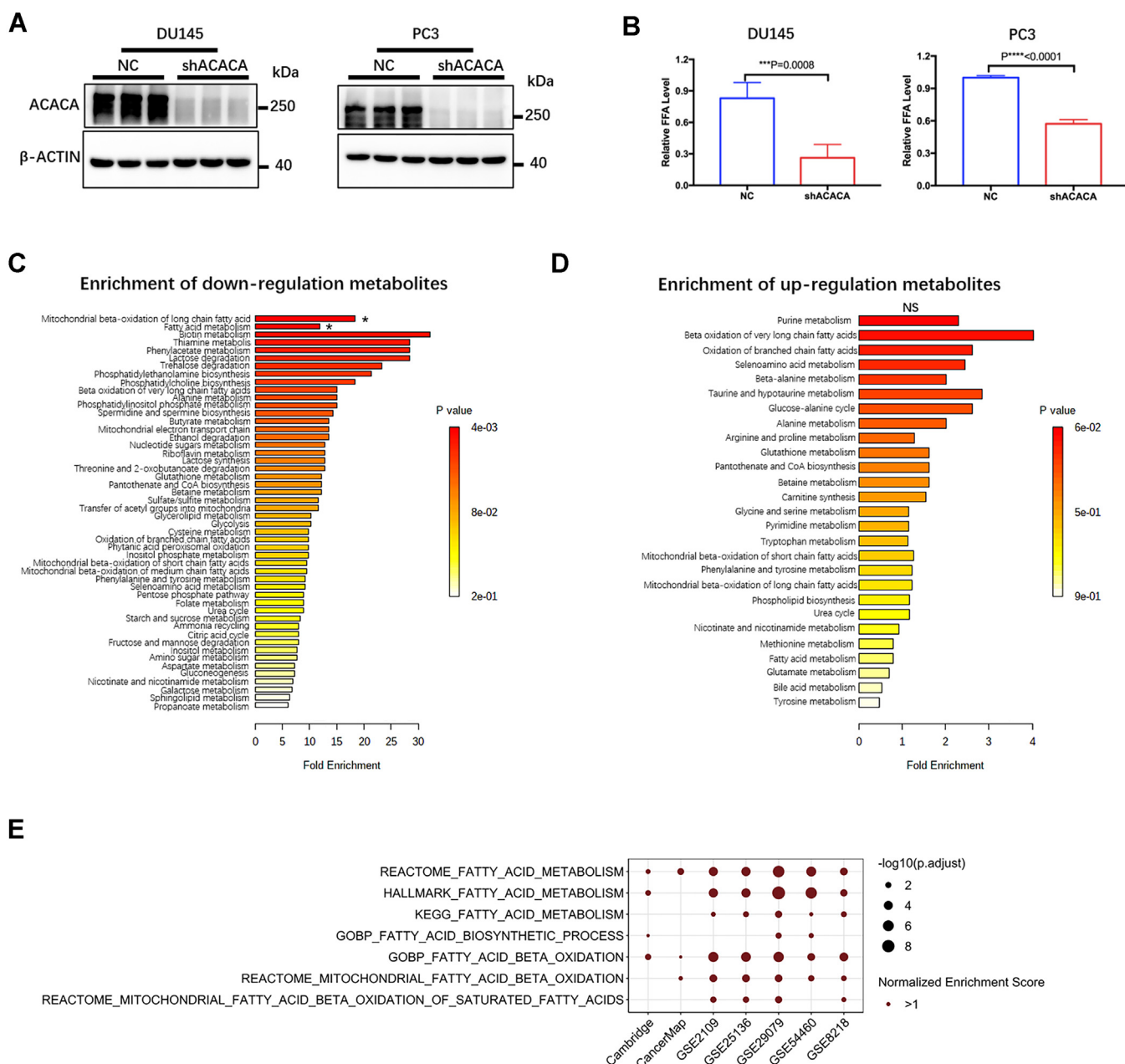
Figure 2. Depletion of ACACA in CRPC cells reduces fatty acid content and suppresses β-oxidation in the mitochondria. *A,* Western blot analysis of ACACA expression in the indicated cell lines. *B,* quantification analysis of cellular free fatty acids in the indicated cell lines. *C* and *D,* metabolic pathway enrichment analysis of metabolites in ACACA knockdown cells. *$*p < 0.05$; NS: not statistically significant ($p > 0.05$). *E,* bubble plot indicates the typical pathways related to ACACA in seven public datasets. Only the statistical significant pathway (adjusted *p*-value < 0.05) is showing. CRPC, castration-resistant prostate cancer.

related genes. FASN, the encoding gene of fatty acid synthase, which is a key enzyme for fatty acid synthesis, showed a coexpression relationship with ACACA in both databases. The relative coexpression coefficient score between ACACA and FASN was 0.686, which was the highest among the 10 genes (Fig. 3, *B–C*). Next, aforementioned seven datasets and CIT dataset were used for GSEA analysis and the result showed that fatty acid synthase activity was statistical significance and pathway activated (Fig. 3*D*). After that, RNA-seq was employed to profile the global changes of ACACA-depletion cells. Bioinformatics analysis indicated that PI3K/AKT signaling pathway was significantly enriched (Fig. 3*F*) and the heatmap

showed that gene related to fatty acid synthesis pathway and PI3K/AKT pathway were downregulated (Fig. 3*E*). Western blot and immunofluorescence staining revealed that FASN expression was downregulated in ACACA-depleted cells (Fig. 3, *G* and *J*). In addition, the levels of phosphorylated ACLY and ACSS2 were also downregulated in ACACA-depleted cells (Fig. 3*G*). ACLY and ACSS2 are both key enzymes of the *de novo* fatty acid synthesis pathway, which are responsible for catalyzing citrate and acetate to acetyl-CoA, respectively, providing the fundamental substrate for *de novo* fatty acid synthesis. As AMPK, PI3K/AKT, and mTOR pathways are involved in modulating the fatty acid synthesis, we detected the
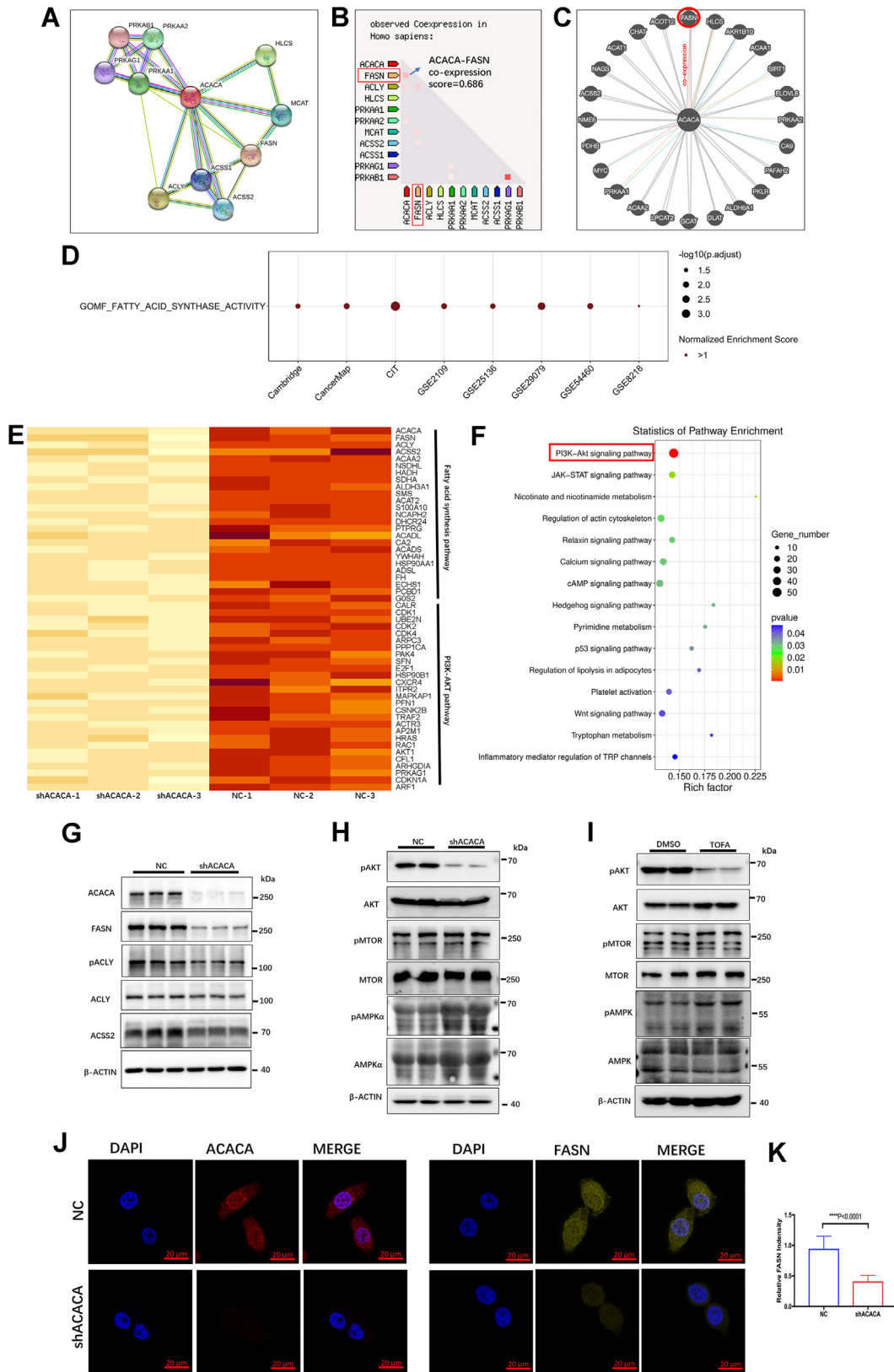
Figure 3. *De novo* synthesis of fatty acids and PI3K/AKT pathway is significantly inhibited in ACACA-depleted cells. *A–C*, ACACA molecular interaction analysis with the Search Tool for the Retrieval of Interacting Genes/Proteins (STRING) and Pathway common database (https://string-db.org and https://apps.pathwaycommons.org). *D*, fatty acid synthase activity was statistical significance in eight datasets. *E* and *F*, fatty acid synthesis pathway and PI3K/AKT pathway were downregulated in the RNA sequence of the ACACA-depletion cells. *G*, Western blot analysis of FASN, ACLY, pACLY, and ACSS2 expression in the ACACA-depletion cells. *H* and *I*, the protein expression level of AMPK alpha, PI3K/AKT, and mTOR pathways in both ACACA-depleted and ACACA inhibitor (TOFA 10 μg/ml, 72 h) treated cells. *J* and *K*, immunofluorescence staining of ACACA and FASN by confocal imaging in the indicated cell lines and quantitative results of relative fluorescence intensity with ImageJ (****$p < 0.0001$).

protein expression level of their activation status. The resulted phosphorylated AKT were downregulated in both ACACA-depleted and ACACA inhibitor, 5-tetradecyloxy-2-furoic acid (TOFA)–treated cells, while phosphorylated AMPK alpha was upregulated conversely. The expression of phosphorylated mTOR and total mTOR were not changed apparently (Fig. 3, *H* and *I*). Furthermore, online data mining also revealed a positive correlation between ACACA and FASN, ACLY, ACSS2, AKT1, AKT2, and AKT3 expression in the clinical sample databases ($p < 0.05$) (Fig. S2). Together, the data suggest that depletion of ACACA effectively reduces the *de novo* fatty acid synthesis of CRPC cells *via* multiple mechanisms.

Depletion of ACACA reduces mitochondrial β-oxidation in CRPC cells

In addition to glucose and glutamine, fatty acids also serve as an energy source, which provides twice as much ATP as carbohydrates through mitochondrial beta-oxidation (8). Metabolomics characterization revealed that metabolites related to mitochondrial beta-oxidation in ACACA-depleted CRPC cells were significantly reduced. The Seahorse Mito-Stress assay showed that the oxygen consumption rate was decreased in ACACA-depleted cells (Fig. 4*A*), together with ATP production, maximal respiration, spare respiratory capacity, proton leak, and basal respiration (Fig. 4, *B–F*). However, the phenotypes aforementioned were almost rescued by the addition of exogenous palmitate. Consistently, similar situation was observed when ACACA was pharmacological inhibition by TOFA (Fig. 4, *G–L*). The results suggest that depletion of ACACA reduces mitochondrial activity. Furthermore, MitoTracker staining showed that the mitochondrial potential was reduced in both ACACA-depleted and TOFA-treated cells, which were also rescued by the addition of exogenous palmitate (Fig. 4, *M–R*).

Carnitine palmitoyltransferase 1 (CPT1) catalyzes the transfer of fatty acid-CoA conjugates to carnitine, an essential step for the mitochondrial uptake of fatty acids and the subsequent beta-oxidation in the mitochondria. Western blotting showed that the expression of CPT1A and CPT1B was downregulated in ACACA-depleted cells (Fig. 4*V*). Mitochondria membrane-localized ACACB allosterically inhibits CPT1 through the production of malonyl-CoA and negatively regulates fatty acid oxidation. The expression of ACACB was increased in ACACA-depleted cells, which synergistically downregulated CPT1 activity and suppressed mitochondrial beta-oxidation (Fig. 4, *S* and *T*). Fatty acid oxidation–derived NADPH is important for cancer cells to maintain NADP$^+$/NADPH homeostasis. As expected, the NADP$^+$/NADPH assay showed that the NADP$^+$/NADPH ratio was increased in ACACA-depleted cells (Fig. 4*U*), which was likely caused by the reduction in mitochondrial beta-oxidation of fatty acids.

Reactive oxygen species and apoptosis are increased in ACACA-depleted cells

According to the RNA-seq profiling analysis, apoptosis pathway was significantly enriched with ACACA-depleted cells (Fig. 5*A*). GSEA analysis with nine datasets showed that expression of ACACA statistically significant suppressed apoptosis pathway (Fig. 5D). Further fluorescence-activated cell sorting (FACS) analysis showed increased apoptosis in ACACA-depleted cells (Fig. 5, *E* and *F*). Consistently, Western blot analysis also showed that depletion of ACACA increased the cleavage of caspase-3 and caspase-9 in CRPC cells (Fig. 5, *B* and *C*). To determine whether depletion of ACACA induced oxidative stress in CRPC cells, CellROX Deep Red dye was used to assess cellular reactive oxygen species (ROS). FACS analysis revealed that the cellular ROS level was increased in ACACA-depleted cells (Fig. 5, *G* and *H*). Consistently, confocal imaging also showed increased ROS staining in ACACA-depleted cells (Fig. 5, *I–L*). Although mitochondria are the major site for the ROS production, the mitochondrial ROS production was decreased in the ACACA-depleted cells. The decreased mitochondrial ROS production was also rescued by the addition of exogenous palmitate, which had similar phenotype with the mitochondrial potential (Fig. S4).

Elevated exogenous lipid uptake compensates for the loss of novel fatty acid synthesis in PCa cells

LDLR, CD36, and SLC27A1 are the three major transporters for the uptake of exogenous fatty acids in cells. TCGA dataset analyses showed that the expression of LDLR, CD36, and SLC27A1 was significantly downregulated in PCa compared with normal prostate tissue (Fig. 6*A*). Quantitative RT-PCR analyses revealed that depletion of ACACA significantly increased the expression of LDLR, CD36, and SLC27A1 in PC3 cells. Consistently, depletion of ACACA also upregulated LDLR expression in DU145 cells, although CD36 and SLC27A1 expression was not significantly different (Fig. 6, *B* and *C*). The data suggest that elevated uptake of exogenous lipid compensates for the loss of novel fatty acid synthesis due to the loss of ACACA. To test this hypothesis, the LDLR expression of ACACA-depleted cells were successfully knockdowned by three LDLR-specific siRNA, then FACS apoptosis analysis showed an increased apoptosis in the LDLR knockdowned ACACA-depleted cells (Fig. 6*D*). Furthermore, cells were cultured in medium containing a reduced concentration of fetal bovine serum (FBS) or delipidated FBS. FACS analysis showed that compared with those cultured in 10% FBS, ACACA-depleted cells cultured in 1% FBS and delipidated FBS had significantly increased apoptosis (Fig. 6*E*). In contrast, very little difference in apoptosis was observed in parental cells cultured in different serum concentrations. However, the apoptosis of the ACACA-depleted cells cultured in delipidated FBS was partially rescued by the addition of exogenous palmitate (Fig. 6*F*).

Blocking of exogenous lipid uptake exacerbated TOFA-induced apoptosis in CRPC cells

TOFA, a potent competitive acetyl-CoA carboxylase inhibitor, which has been widely proven in inhibiting fatty acid synthesis. To verify the phenotype aforementioned, TOFA was employed as pharmacological inhibition of ACACA. PC3 or DU145 WT
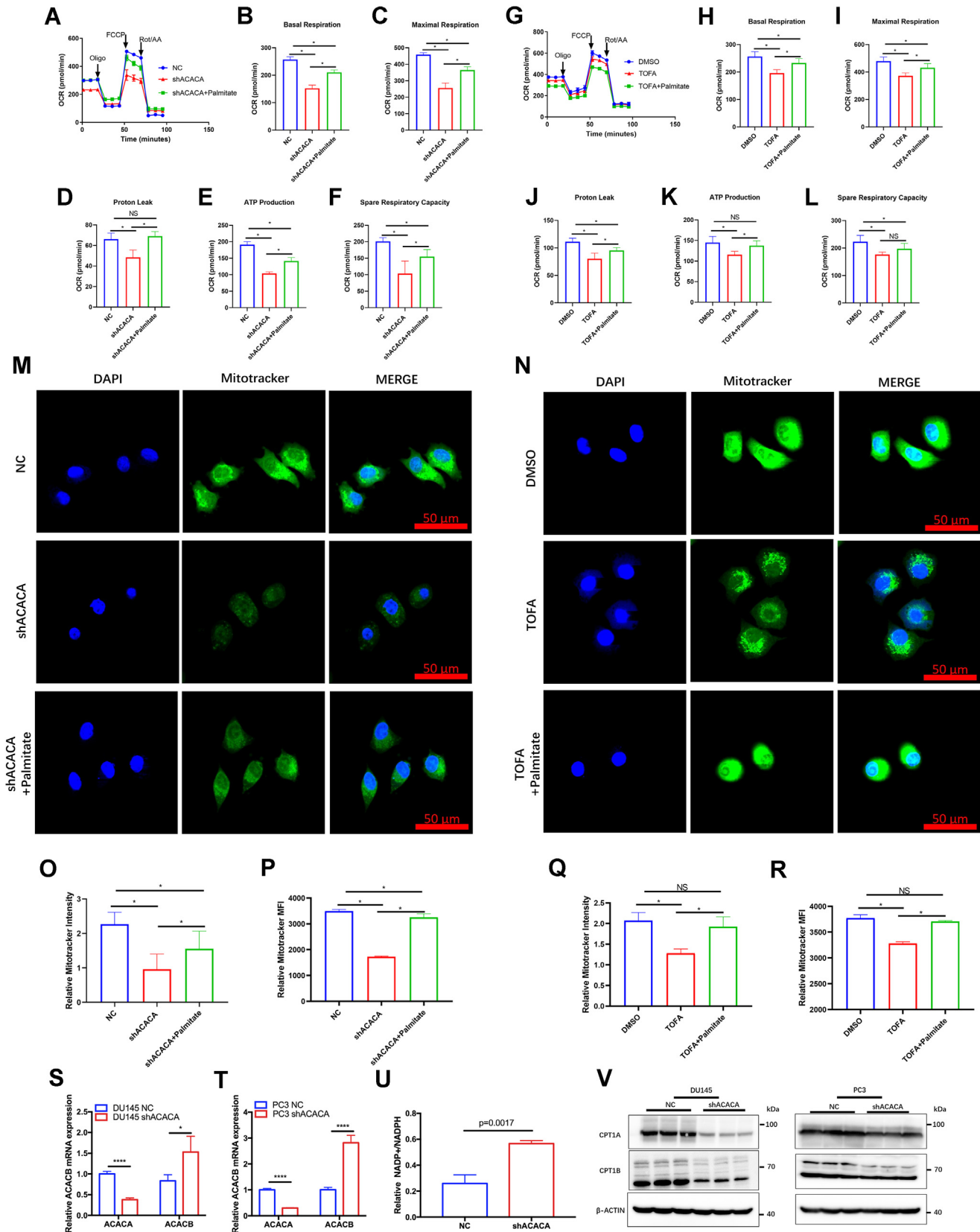
Figure 4. Depletion of ACACA reduces mitochondrial β-oxidation in CRPC cells. *A–L*, depletion of ACACA reduces mitochondrial activity, and the phenotypes could be rescued by the addition of exogenous palmitate (100 μM, 72 h). The same results are shown in TOFA-treated cells (10 μg/ml). *M–R*, MitoTracker staining showed that the mitochondrial potential was reduced in both ACACA-depleted and TOFA-treated cells, rescued by the addition of exogenous palmitate. *S–T*, the mRNA expression of ACACB was increased in ACACA-depleted cells. *U*, the NADP+/NADPH ratio was increased in ACACA-depleted cells. *V*, Western blotting showed that the expression of CPT1A and CPT1B was downregulated in ACACA-depleted cells. (*$p < 0.05$); NS: not statistically significant ($p > 0.05$).
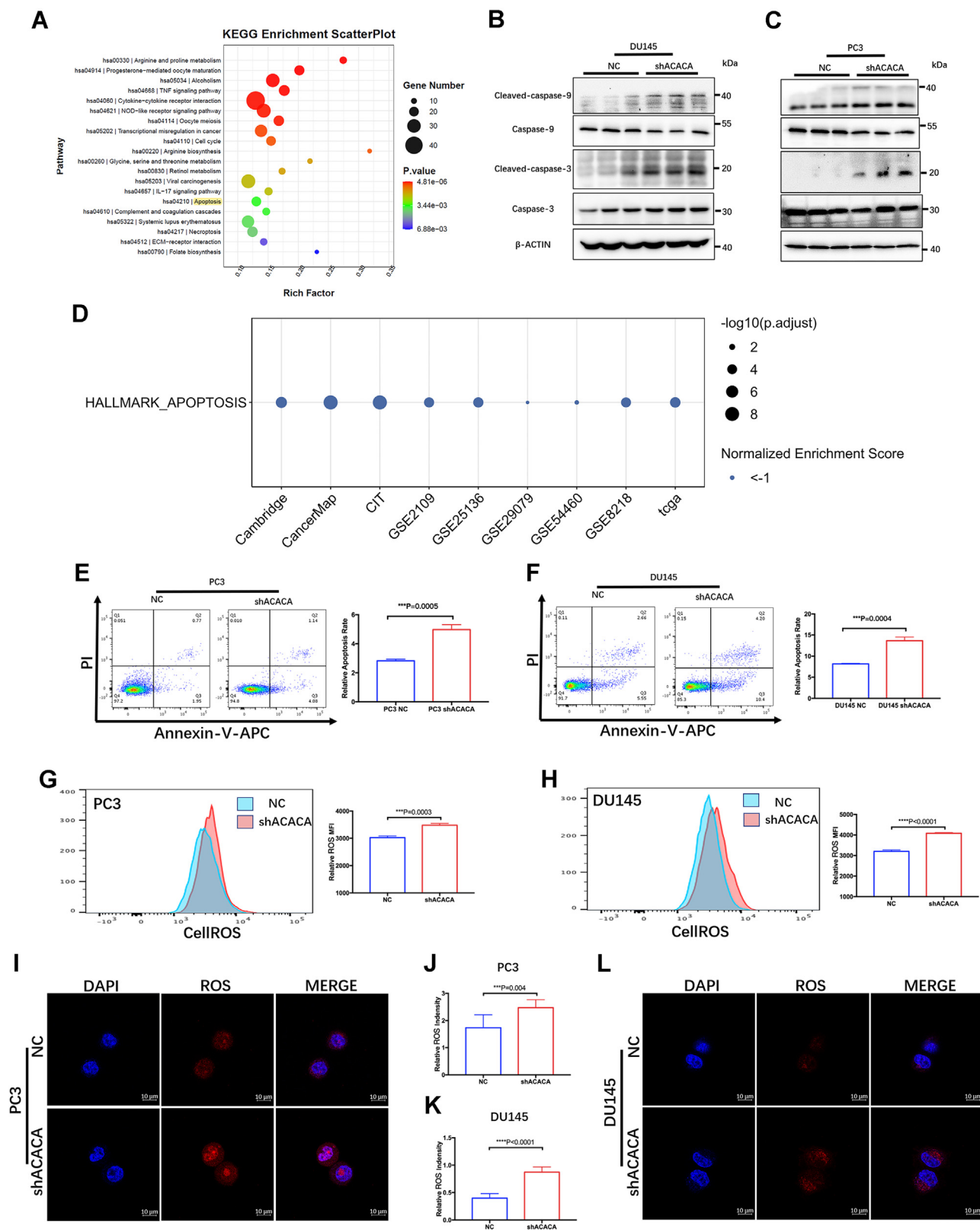
Figure 5. Reactive oxygen species (ROS) and apoptosis are increased in ACACA-depleted cells. *A*, apoptosis pathway was enriched with ACACA-depleted cells according to the RNA-seq profiling analysis. *B* and *C*, Western blot analysis showed that depletion of ACACA increased the cleavage of caspase-3 and caspase-9 in CRPC cells. *D*, expression of ACACA suppressed apoptosis pathway in nine public datasets. *E* and *F*, FACS analysis of apoptosis and quantitative results. *G* and *H*, FACS analysis of cellular ROS and quantitative analyses of relative fluorescence intensity. *I–L*, confocal imaging of cellular ROS and quantitative analyses of relative fluorescence intensity. FACS, fluorescence-activated cell sorting.
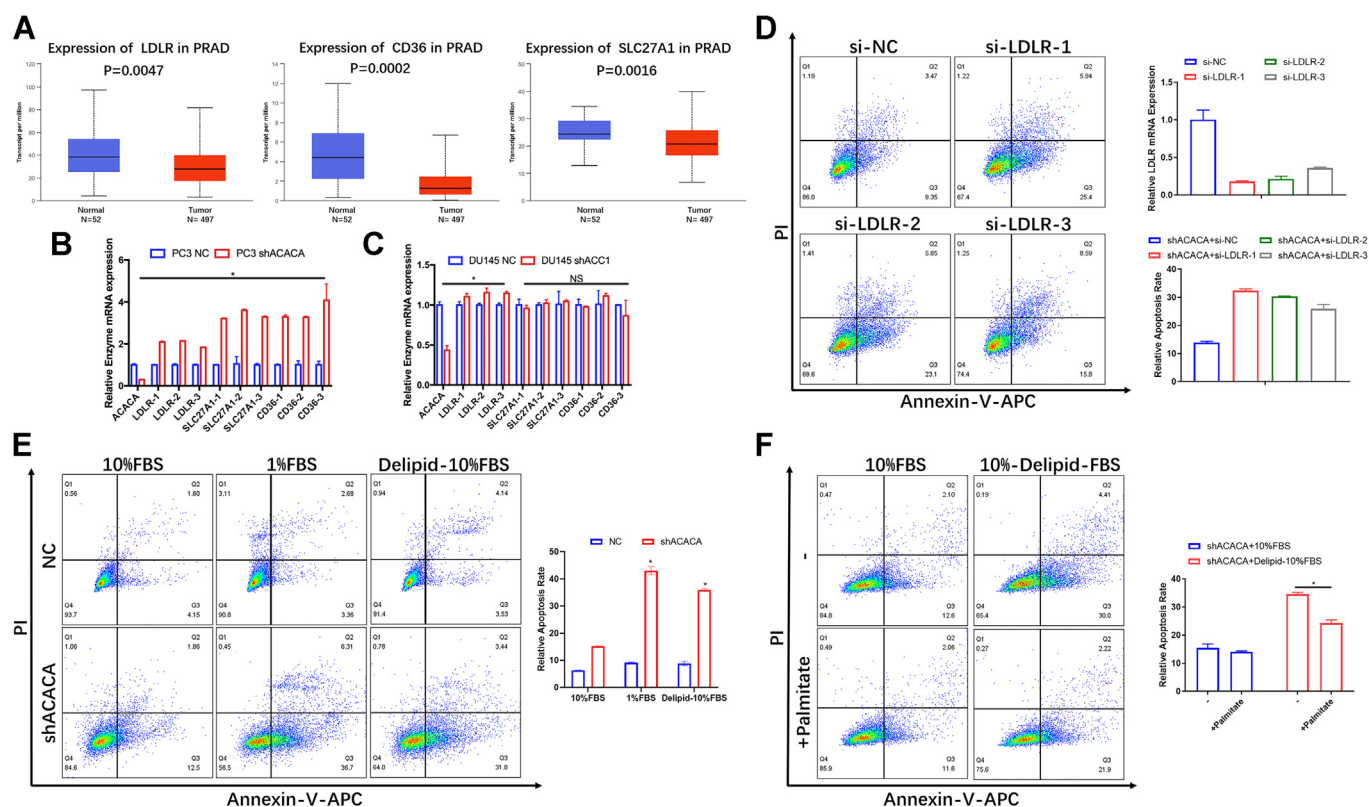
Figure 6. Elevated exogenous lipid uptake compensates for the loss of novel fatty acid synthesis in PCa cells. *A*, relative expression of LDLR, CD36, and SLC27A1 in the TCGA PCa dataset. *B* and *C*, qPCR analysis of ACACA, LDLR, CD36, and SLC27A1 mRNA expression in the indicated cell lines. *D*, FACS analysis of apoptosis in the LDLR knockdowned ACACA-depleted PCa cells. *E*, FACS analysis of PCa cell apoptosis cultured in medium with different serum concentrations or delipidated FBS, and (*F*) the apoptosis were partially rescued by the addition of exogenous palmitate (100 μM, 72 h). *p < 0.05. FACS, fluorescence-activated cell sorting; FBS, fetal bovine serum; qPCR, quantitative PCR.

cells were cultured in medium containing 10% FBS or 1% FBS or delipidated FBS, then cotreated with 0 μg/ml, 5 μg/ml, or 10 μg/ml TOFA and 0 μM or 100 μM palmitate for 72 h. Consistently, FACS analysis showed that compared with those cultured in 10% FBS, TOFA-treated cells cultured in 1% FBS and delipidated FBS had significantly increased apoptosis (Figs. 7, *B* and *C* and S3, *B* and *C*). The cells cultured in 1% FBS or delipidated FBS medium with 10 μg/ml TOFA treatment were almost dead (Figs. 7*A* and S3*A*). In addition, Western blot analysis showed an increased cleaved PPAR expression with the TOFA-treated cells, especially in 1% FBS and delipidated FBS groups. By contrast, phosphory-lated AKT expression was downregulated in those cells. Furthermore, confocal imaging showed an increased fluorescence intensity with the TOFA-treated cells, especially in 1% FBS and delipidated FBS groups (Fig. 7*E*).

Discussion

Cancer cells frequently have an elevated capacity for *de novo* fatty acid synthesis to meet the needs of rapid cell proliferative tumors. PCa is no exception, which makes it susceptible to treatment to suppress fatty acid synthesis (11–13, 22). In fact, many potential targets related to fatty acid synthesis have been explored thus far, including FASN, ACLY, and ACSS2 (23). However, most efforts have been focused on FASN, although it has been reported that ACACA expression is elevated in breast

cancer, liver cancer, lung cancer, and prostate cancer (15–17, 19). Herein, we report that ACACA was highly expressed in PCa, especially in CRPC, and patients with higher ACACA expression had shorter disease-free survival times. Depletion of ACACA in CRPC cells inhibited *de novo* synthesis of fatty acids and PI3K/AKT pathway, suppressed proliferation and tumorigenesis, reduced mitochondrial beta oxidation, and increased ROS and apoptosis. We also reported that depletion of ACACA decreased the expression of FASN, ACLY, and ACSS2, the key enzymes for *de novo* fatty acid synthesis. Furthermore, we reported that reduced lipid or serum supplementation exacerbated apoptosis induced by ACACA depletion, suggesting that exogenous lipid uptake likely compensated for the loss of novel fatty acid synthesis in PCa cells. Therefore, suppression of lipid uptake is needed to improve the efficacy of blocking *de novo* synthesis therapy for PCa.

In this study, we found that depletion of ACACA in CRPC cells inhibited mitochondrial function and reduced ATP production. Metabolomics analysis showed that the reduced metabolites in ACACA-depleted CRPC cells were enriched in the mitochondria beta-oxidation of the long-chain fatty acid synthesis pathways. Our data indicate that compensatory expression of ACACB located at the mitochondrial outer membrane is likely the causal factor of CPT1 inhibition in ACACA-depleted cells (7, 24, 25). Consequently, decreased expression of the fatty
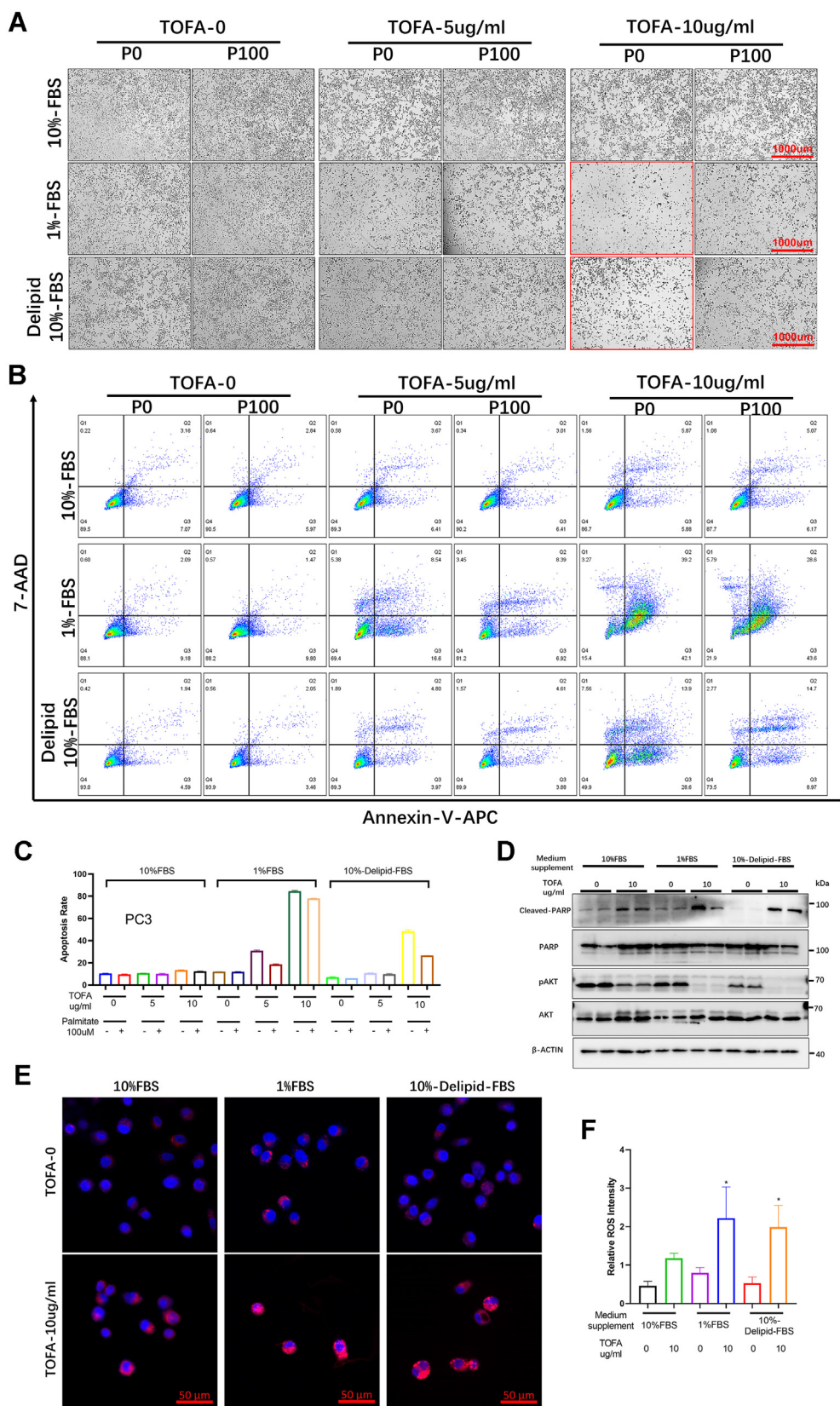
Figure 7. Blocking of exogenous lipid uptake exacerbated TOFA-induced apoptosis in CRPC cells. *A*, cells images of the CRPC cells cultured in 1% FBS or delipidated FBS medium with 10 μg/ml TOFA treatment. *B–D*, FACS analysis and WB showed the apoptosis in above cell culture conditions. *E* and *F*, confocal imaging of cellular ROS and quantitative analyses of relative fluorescence intensity. *$p < 0.05$. CRPC, castration-resistant prostate cancer; FACS, fluorescence-activated cell sorting; FBS, fetal bovine serum; ROS, reactive osygen species; WB, Western blotting.

acid transporter CPT1 will reduce the delivery of fatty acids to mitochondria for beta-oxidation, resulting in weakened mitochondrial function and increased energy stress in ACACA-depleted CRPC cells. Together with the imbalance of NADP+/NADPH, increased energy stress will induce elevation of the ROS level in the cells and lead to cell apoptosis.

Our data revealed that diminishing ACACA-mediated *de novo* fatty acid synthesis induced cell damage and that depletion of ACACA increased the dependency on serum lipid supplementation in cell culture. The results suggest that the deficiency in *de novo* fatty acid synthesis in CRPC cells can be rescued by increasing the uptake of exogenous fatty acids, which is likely the mechanism by which cancer cells resist treatment to block *de novo* fatty acid synthesis (23). Our results that depletion of ACACA led to increased expression of the lipid transporters exogenous LDLR, SLC27A1, and CD36 further support this notion. Therefore, lower serum lipid levels and inhibited lipid uptake can be an effective venue to increase the efficacy of ACACA-targeted therapy for PCa.

In summary, ectopic expression of ACACA in PCa cells reduces the dependence on exogenous fatty acids, which are needed for fast membrane synthesis in PCa cells. Suppression of ACACA, together with blocking exogenous fatty acid uptake, will be a novel therapeutic strategy for currently uncurable CRPC (Fig. 8).

Experimental procedures

Cell culture

The human PCa cell lines DU145 and PC3 were purchased from the American Type Culture Collection and cultured in Dulbecco's modified Eagle's medium (DMEM) (Gibco, C11995500CP) supplemented with 10% FBS (Gibco, 10270-106) or 10% lipid-depleted FBS (VivaCell, C3840-0100), and 1% antibiotics (penicillin-streptomycin, Gibco, 15140122). The cells were incubated in a 5% CO_2 incubator at 37 °C. The acetyl-CoA carboxylase inhibitor TOFA (abcam, ab141578) and palmitate acid (Macklin, p815428) was utilized in the cell culture.

The ACACA-specific shRNA and control vector were purchased from HYY Med Company. The shRNA sequence was TACAAGGGATACAGGTATTTA. The plasmid contains sequences encoding puromycin resistance protein, GFP, and shRNA. Two days after infection with the lentivirus, the infected cells were selected by growing in medium containing 2 mg/ml puromycin. Single clones of transfected cells were selected for verification and analyses. In addition, we seeded $1 \times 10_{-}5$ cells in 6-well plates for fusion of 50% to 60% for 24 h; then, cells were transfected with siRNAs mixed with siRNA-Mate (GenePharm, G04002) for 72 h and transfection efficiency was verified *via* reverse transcription quantitative PCR. The sequences used for siRNA are listed in Table S1.

Bioinformatic analysis

TCGA and Taylor datasets were downloaded from https://xenabrowser.net/datapages/, the GSE70768 dataset was downloaded from the GEO database, and the fatty acid metabolism gene set was downloaded from the website https://www.gsea-msigdb.org/gsea/index.jsp. The three datasets were analyzed for the differential expression of key genes related to fatty acid metabolism. The correlation coefficient between the target gene and each other gene in TCGA was first calculated by Pearson correlation analysis. Then, the obtained gene list was ordered *via* the decreasing levels of the correlation coefficient. The ordered gene list was further fitted in GSEA by the R package 'Cluster Profilter' using the annotation of 'hallmark gene sets'. A false discovery rate <0.25 and adjusted *p* value < 0.01 were considered statistically significant.

The profiling data of mRNAs and clinical characteristics for 495 PCa patients from the TCGA-PRAD project were downloaded and processed in the R package GDCRNAtools. The mRNA expression data in seven public datasets (Cambridge, CancerMap, GSE21019, GSE25136, GSE29079, GSE54460, GSE8218) were acquired from the GEO (https://www.ncbi.nlm.nih.gov/geo/).

GSEA: To discover the potential biological pathways related to ACACA in PCa, differentially expressed analysis was firstly
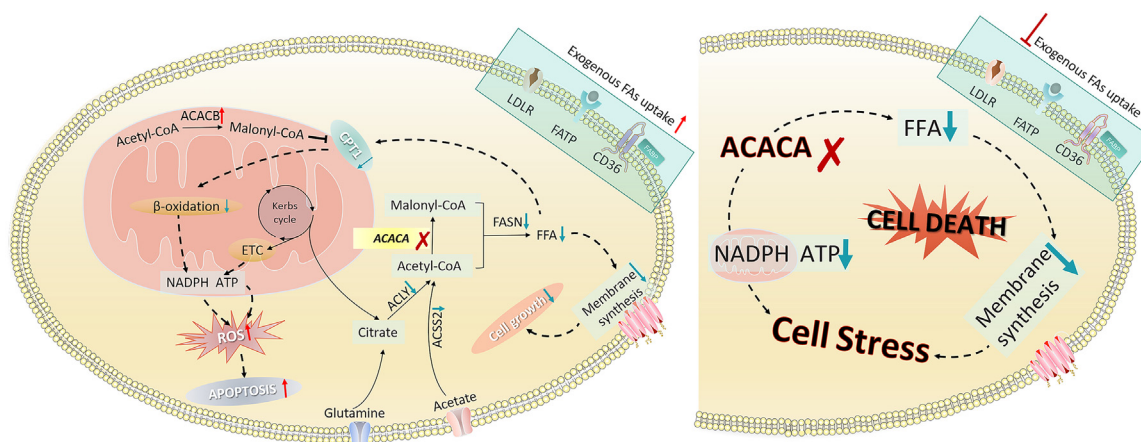

Figure 8. Model illustrating that inhibition of *de novo* fatty acid synthesis in castration-resistant prostate cancer cells by depleting acetyl-CoA carboxylase 1 suppresses mitochondrial β-oxidation, leading to reduced proliferation and increased apoptosis, which is exacerbated by insufficient exogenous fatty acid uptake.

performed between high- and low-expression subgroup based on the median expression levels of ACACA in each dataset. Then, the genes were ranked *via* the decreasing levels of Log2Foldchange. The ordered gene list was further fitted into GSEA by R package 'clusterProfilter'. Adjusted *p*-value < 0.05 and normalized enrichment score (NES) >1 were considered as statistical significance and pathway activated. Adjusted *p*-value < 0.05 and normalized enrichment score (NES) <−1 were considered as statistical significance and pathway suppressed.

Histology

Prostate tissues and xenografts were fixed, embedded, and sectioned as described (26). The antigen epitopes were retrieved by microwave heating in citric acid antigen repair solution. Immunohistochemical staining was performed using an UltraSensitive SP kit (MXB, #KIT-9710) according to the user manual. Tumor samples were stained with the following primary antibodies: ACC1 (CST, #3662). The slides were stained with 3,3′-diaminobenzidine substrate (MXB, #DAB-0031), counterstained with hematoxylin, and mounted in mounting medium.

Free fatty acid quantitation assay

Cells (1×10^6) were homogenized in 200 μl of 1% (w/v) Triton X-100-chloroform (RATIO) solution. After centrifugation at 13,000*g* for 10 min, the organic phases (lower phase) of the supernatant were collected and air dried at 50 °C to remove chloroform. The samples were then vacuum dried for 30 min and dissolved in 200 μl of fatty acid assay buffer by vortexing extensively for 5 min. The sample volumes were brought to 50 μl with fatty acid assay buffer. ACS reagent and Master Reaction Mix were added to each sample according to the instructions of the Free Fatty Acid Quantitation Kit (catalog number MAK044, Sigma–Aldrich). The samples were incubated for 30 min at 37 °C in the dark. The absorbance at 570 nm (A_{570}) was measured.

Metabolite analysis

The metabolite profiles of the cells were determined by LC/MS (21). Both downregulated and upregulated metabolites were analyzed on the Metabolite Set Enrichment analysis website for related profiling (https://dev.metaboanalyst.ca/MetaboAnalyst/upload/EnrichUploadView.xhtml).

Quantitative real-time PCR

Total RNA from tumor cells was extracted with the RNA extraction reagent NucleoZol (MN, #740404.200) according to the user's manual. RNA quality and concentration were determined by spectrophotometer. RNA samples were reverse transcribed into complementary DNA (cDNA) using HiScript III Reverse Transcriptase (Vazyme, # R323-01) according to the product guide. The cDNAs were mixed with 2 × volumes of ChamQ Universal SYBR qPCR Master Mix (Vazyme, #Q711) and analyzed with a 96-well real-time PCR machine. Expression was normalized to that of GAPDH. The primer

sequences used for quantitative (q)RT-PCR are listed in Table S1.

Western blot analysis

Cell samples were lysed in radioimmunoprecipitation assay buffer (BoCai Biology, #R0127) in the presence of 100× PMSF (Beyotime, #ST506) protease inhibitor and 50× phosphatase inhibitor (BoCai Biology, #R0127). The gels for protein electrophoresis were prepared using the SDS-PAGE Gel Preparation Kit 1 (Beyotime, #P0012A). The samples separated by SDS-PAGE were electrotransferred to polyvinylidene fluoride membranes for 100 min at 300 mA. The membranes were blocked for 10 min using NcmBlot blocking buffer (NCM Biotech, #P30500) and incubated overnight at 4 °C with the primary antibody diluted in tris-buffered saline with Tween 20 (TBST) with bovine serum albumin (5% w/v). After washing with TBST three times, the membranes were incubated with the secondary antibody for 1 h at room temperature (RT). After washing three times with TBST to remove nonspecific binding, the membranes were incubated in chemiluminescent reagents (Millipore, #WBKLS0100). The images were captured with X-ray films, which were scanned with a densitometer for quantitation. The antibody information is listed in Table S2.

Immunofluorescence

Cells were seeded in confocal plates and incubated at 37 °C for at least one night prior to analyses. The cells were fixed with 4% formaldehyde and then incubated with 0.5% Triton X-100. After incubation with the primary antibodies overnight at 4 °C, the cells were washed three times with PBS and then incubated with the secondary antibody (Alexa Fluor, Boster) at RT for 1 h. After washing, the cells were incubated with diamidino-2-phenylindole for 5 min. The images were taken by a confocal laser scanning microscope (LSM880, Leica). Fluorescence intensity was quantified by ImageJ software (Java).

Reactive oxygen species detection

Cells were seeded in 6-well plates at least one night prior to the analyses. The cells were then incubated with dihydroethidium (Beyotime Biotechnology, S0033) or MitoSOX Mitochondrial Superoxide Indicators (Invitrogen, M36008) at 37 °C in a CO_2 incubator (avoiding light) for 30 min. The cells were then washed three times in serum-free cell culture medium. One well of each treatment was digested with trypsin for the preparation of a single-cell suspension to be analyzed with a flow cytometer. The other wells were then incubated with Hoechst 33342 for 30 min before confocal imaging. FlowJo (Becton, Dickinson and Company) and ImageJ software were employed to quantify the cell numbers and fluorescence intensity, respectively.

MitoTracker assay

Two sets of cells were seeded in 6-well plates and cultured at 37 °C for at least one night in advance. MitoTracker Red (Life Technologies, M7512) was added to the cells. After incubation at 37 °C with CO_2 (avoiding light) for 30 min, the cells were then incubated with Hoechst 33342 for 30 min

before confocal imaging. One well for each sample was digested into a single cell suspension for flow cytometry analyses. FlowJo and ImageJ software were employed to quantify the cell number and fluorescence intensity, respectively.

Seahorse assay

The Seahorse Fe 24 Extracellular Flux Bioanalyzer (Agilent) was used to measure the oxygen consumption rate with the Mitostress kit according to the manufacturer's protocol. Cells (30,000 per well) were seeded into specific culture plates in complete medium overnight. The culture medium was then changed to fresh DMEM containing 10 mM glucose, 2 mM L-glutamine, and 1 mM sodium pyruvate and incubated for 1 h. After incubation in a CO_2-free incubator to guarantee precise measurements of extracellular pH, oligomycin (Oligo, 1 mM), carbonyl cyanide 4-trifluoromethoxy-phenylhydrazone (FCCP) (1 mM), and rotenone/antimycin A (Rot/AA, 1 mM) were sequentially loaded into each well. The Seahorse assay was run in an XFe24 Extracellular Flux Analyzer (Agilent Technologies). The results were analyzed using Wave program 2.6.0 (Seahorse Bioscience).

Apoptosis assay

A total of 1×10^6 cells were stained with an Annexin V-APC/7-AAD apoptosis kit (MultiSciences, #AP105) according to the user's manual. Then, the stained apoptotic cells were detected by a flow cytometer. FlowJo software was employed to quantify the apoptosis rate.

NADP/NADPH assay

The NADP+/NADPH colorimetric detection kit was purchased from Beyotime, #S0179. We conducted experiments according to the manufacturer's instructions. A total of 1×10^6 cells were seeded in a 6-cm dish and cultured for 24 h. After removing the culture medium, 200 μl of NADP+/NADPH extract buffer was added to each well. The lysates were collected for centrifugation at $12,000g$ and 4 °C for 10 min to remove the insoluble fractions. The supernatant was collected for the analyses. The NADPH standard and G6PDH working solutions were prepared according to the instruction manual. The supernatants (100 μl) were transferred to a centrifuge tube and heated in a water bath (60 °C) to decompose NADP+. Blank control, NADPH standard, and samples were loaded in a 96-well plate. The G6PDH working solution (100 μl) was added to each well and mixed gently. The plates were incubated at 37 °C (protected from light) for 10 min. The developing solution (10 μl) was then added to each well. After incubation at 37 °C for 15 min (protected from light), the absorbance at 450 nm was measured. The NADP+/NADPH ratio was determined according to the instructions.

RNA extraction and library construction

TRIzol reagent (Invitrogen) following the manufacturer's procedure was utilized to extract the RNA of cells and tissues. The RNA amount and purity of each sample was quantified using NanoDrop ND-1000 (NanoDrop); poly(A)- or poly(A)+ RNA fragments were broken into small pieces by divalent cations at a high temperature. The final cDNA library was constructed from cDNA reverse transcribed from the cleaved small RNA fragments. We performed the paired-end sequencing (PE150) on an illumina Novaseq 6000 (LC-Bio Technology Co, Ltd) following the vendor's recommended protocol.

Bioinformatics analysis of RNA-seq

The sequence quality was also verified using fastp software (https://github.com/OpenGene/fastp). We used HISAT2 (https://ccb.jhu.edu/software/hisat2) to map reads to the reference genome of *Homo sapiens* GRCh38. The mapped reads of each sample were assembled using StringTie (https://ccb.jhu.edu/software/stringtie). Then, all transcriptomes from all samples were merged to reconstruct a comprehensive transcriptome using gffcompare (https://github.com/gpertea/gffcompare/). StringTie was used to perform expression level for mRNAs by calculating FPKM (FPKM = [total_exon_fragments/mapped_reads(millions) × exon_length(kB)]). The differentially expressed mRNAs were selected with fold change >2 or fold change <0.5 and with parametric F-test comparing nested linear models (p value < 0.05) by R package edgeR (https://bioconductor.org/packages/release/bioc/html/edgeR.html).

Statistical analysis

All experiments were performed at least three times. GraphPad software (GraphPad Software Inc) was used for statistical analysis. Data analyses were performed using the independent two-tailed t test, and the error bars indicate the mean ± SD. $p < 0.05$ was considered statistically significant.

Data availability

All the data are available either in the main article or in the supporting document.

GSEA, gene set enrichment analysis; mCRPC, metastatic castration-resistant PCa; PCa, prostate cancer; ROS, reactive oxygen species; TCGA, The Cancer Genome Atlas.

References

1. Sung, H., Ferlay, J., Siegel, R. L., Laversanne, M., Soerjomataram, I., Jemal, A., *et al*. (2021) Global cancer statistics 2020: GLOBOCAN estimates of incidence and mortality Worldwide for 36 cancers in 185 countries. *CA. Cancer J. Clin.* **71**, 209–249
2. Siegel, R. L., Miller, K. D., Fuchs, H. E., and Jemal, A. (2022) Cancer statistics, 2022. *CA. Cancer J. Clin.* **72**, 7–33
3. Cooperberg, M. R., and Carroll, P. R. (2015) Trends in management for patients with localized prostate cancer, 1990-2013. *JAMA* **314**, 80–82
4. Sandhu, S., Moore, C. M., Chiong, E., Beltran, H., Bristow, R. G., and Williams, S. G. (2021) Prostate cancer. *Lancet* **398**, 1075–1090
5. DeBerardinis, R. J., and Chandel, N. S. (2016) Fundamentals of cancer metabolism. *Sci. Adv.* **2**, e1600200
6. Hanahan, D., and Weinberg, R. A. (2011) Hallmarks of cancer: the next generation. *Cell* **144**, 646–674
7. Currie, E., Schulze, A., Zechner, R., Walther, T. C., and Farese, R. V., Jr. (2013) Cellular fatty acid metabolism and cancer. *Cell. Metab.* **18**, 153–161
8. Carracedo, A., Cantley, L. C., and Pandolfi, P. P. (2013) Cancer metabolism: fatty acid oxidation in the limelight. *Nat. Rev. Cancer* **13**, 227–232
9. Ookhtens, M., Kannan, R., Lyon, I., and Baker, N. (1984) Liver and adipose tissue contributions to newly formed fatty acids in an ascites tumor. *Am. J. Physiol.* **247**, R146–R153
10. Rossi, S., Graner, E., Febbo, P., Weinstein, L., Bhattacharya, N., Onody, T., *et al*. (2003) Fatty acid synthase expression defines distinct molecular signatures in prostate cancer. *Mol. Cancer Res.* **1**, 707–715
11. Zadra, G., Photopoulos, C., Tyekucheva, S., Heidari, P., Weng, Q. P., Fedele, G., *et al*. (2014) A novel direct activator of AMPK inhibits prostate cancer growth by blocking lipogenesis. *EMBO. Mol. Med.* **6**, 519–538
12. Singh, K. B., Kim, S. H., Hahm, E. R., Pore, S. K., Jacobs, B. L., and Singh, S. V. (2018) Prostate cancer chemoprevention by sulforaphane in a preclinical mouse model is associated with inhibition of fatty acid metabolism. *Carcinogenesis* **39**, 826–837
13. De Schrijver, E., Brusselmans, K., Heyns, W., Verhoeven, G., and Swinnen, J. V. (2003) RNA interference-mediated silencing of the fatty acid synthase gene attenuates growth and induces morphological changes and apoptosis of LNCaP prostate cancer cells. *Cancer Res.* **63**, 3799–3804
14. Wakil, S. J., and Abu-Elheiga, L. A. (2009) Fatty acid metabolism: target for metabolic syndrome. *J. Lipid. Res.* **50**, S138–S143
15. Svensson, R. U., Parker, S. J., Eichner, L. J., Kolar, M. J., Wallace, M., Brun, S. N., *et al*. (2016) Inhibition of acetyl-CoA carboxylase suppresses fatty acid synthesis and tumor growth of non-small-cell lung cancer in preclinical models. *Nat. Med.* **22**, 1108–1119
16. Chajès, V., Cambot, M., Moreau, K., Lenoir, G. M., and Joulin, V. (2006) Acetyl-CoA carboxylase alpha is essential to breast cancer cell survival. *Cancer Res.* **66**, 5287–5294
17. Lally, J., Ghoshal, S., DePeralta, D. K., Moaven, O., Wei, L., Masia, R., *et al*. (2019) Inhibition of acetyl-CoA carboxylase by phosphorylation or the inhibitor ND-654 suppresses lipogenesis and hepatocellular carcinoma. *Cell. Metab.* **29**, 174–182.e5
18. Jeon, S. M., Chandel, N. S., and Hay, N. (2012) AMPK regulates NADPH homeostasis to promote tumour cell survival during energy stress. *Nature* **485**, 661–665
19. Rios Garcia, M., Steinbauer, B., Srivastava, K., Singhal, M., Mattijssen, F., Maida, A., *et al*. (2017) Acetyl-CoA carboxylase 1-dependent protein acetylation controls breast cancer metastasis and recurrence. *Cell. Metab.* **26**, 842–855.e5
20. Brusselmans, K., De Schrijver, E., Verhoeven, G., and Swinnen, J. V. (2005) RNA interference-mediated silencing of the acetyl-CoA-carboxylase-alpha gene induces growth inhibition and apoptosis of prostate cancer cells. *Cancer Res.* **65**, 6719–6725
21. Zhang, H., Liu, S., Cai, Z., Dong, W., Ye, J., Cai, Z., *et al*. (2021) Downregulation of ACACA suppresses the malignant progression of prostate cancer through inhibiting mitochondrial potential. *J. Cancer* **12**, 232–243
22. Menendez, J. A., Mehmi, I., Papadimitropoulou, A., Vander Steen, T., Cuyàs, E., Verdura, S., *et al*. (2020) Fatty acid synthase is a key enabler for endocrine resistance in Heregulin-overexpressing luminal B-like breast cancer. Int. *J. Mol. Sci.* **21**, 7661
23. Röhrig, F., and Schulze, A. (2016) The multifaceted roles of fatty acid synthesis in cancer. *Nat. Rev. Cancer* **16**, 732–749
24. Schlaepfer, I. R., Rider, L., Rodrigues, L. U., Gijón, M. A., Pac, C. T., Romero, L., *et al*. (2014) Lipid catabolism via CPT1 as a therapeutic target for prostate cancer. *Mol. Cancer Ther.* **13**, 2361–2371
25. McGarry, J. D., Leatherman, G. F., and Foster, D. W. (1978) Carnitine palmitoyltransferase I. The site of inhibition of hepatic fatty acid oxidation by malonyl-CoA. *J. Biol. Chem.* **253**, 4128–4136
26. Liu, J., Chen, G., Liu, Z., Liu, S., Cai, Z., You, P., *et al*. (2018) Aberrant FGFR tyrosine kinase signaling enhances the warburg effect by reprogramming LDH isoform expression and activity in prostate cancer. *Cancer Res.* **78**, 4459–4470

ASBMB